ACS APPLIED MATERIALS & INTERFACES

Research Article

www.acsami.org

Improved Photoelectrochemical Activity of $CaFe_2O_4/BiVO_4$ Heterojunction Photoanode by Reduced Surface Recombination in Solar Water Oxidation

Eun Sun Kim,[†,§] Hyun Joon Kang,[†,§] Ganesan Magesh,[‡] Jae Young Kim,[‡] Ji-Wook Jang,[‡] and Jae Sung Lee*[,‡]

[†]Department of Chemical Engineering, Pohang University of Science and Technology (POSTECH), 77 Cheongam-ro, Nam-gu, Pohang 790-784, Republic of Korea

[‡]School of Energy and Chemical Engineering, Ulsan National Institute of Science and Technology (UNIST), 50 UNIST-gil, Ulsan 689-798, Republic of Korea

Supporting Information

ABSTRACT: A bismuth vanadate photoanode was first fabricated by the metal−organic decomposition method and particles of calcium ferrite were electrophoretically deposited to construct a heterojunction photoanode. The characteristics of the photoanodes were investigated in photoelectrochemical water oxidation under simulated 1 sun (100 mW cm^{-2}) irradiation. Relative to the pristine $BiVO_4$ anode, the formation of the heterojunction structure of $CaFe_2O_4/BiVO_4$ increased the photocurrent density by about 60%. The effect of heterojunction formation on the transfer of charge carriers was investigated using hydrogen peroxide as a hole scavenger. It was demonstrated that the heterojunction formation reduced the charge recombination on the electrode surface with little effect on bulk recombination. The modification with an oxygen evolving catalyst, cobalt phosphate (Co-Pi), was also beneficial for improving the efficiency of $CaFe_2O_4/BiVO_4$ heterojunction photoanode mainly by increasing the stability.

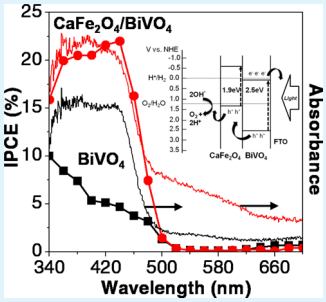

KEYWORDS: *bismuth vanadate, calcium ferrite, heterojunction photoanode, photoelectrochemical cell, water splitting*

1. INTRODUCTION

Solar energy conversion to hydrogen is an ideal method to supply a clean and sustainable fuel. The hydrogen is a carbon-neutral fuel that emits only water as a combustion product and it has a high energy output per unit weight (123 MJ/kg). The photoelectrochemical (PEC) cell is a highly promising system to produce hydrogen and oxygen from water using solar energy. Since the first demonstration of the concept,[1] photocatalytic semiconductor materials have been intensively sought that could utilize sunlight for water splitting with a high efficiency. The simple metal oxides such as WO_3[2,3] and Fe_2O_3[4,5] are popular candidate photocatalytic materials because of their visible light activity, stability in aqueous electrolyte and low cost. Monoclinic bismuth vanadate ($BiVO_4$) is a highly active photocatalyst for oxygen evolution under visible light with its band gap of 2.4−2.5 eV.[6,7] The valence band position of $BiVO_4$ is suitable for water oxidation and consists of O 2p and Bi 6s hybrid orbitals, whereas the position of the conduction band composed of V 3d orbitals is slightly more positive than the hydrogen evolution potential and does not allow hydrogen evolution.[8]

The photocatalytic properties of $BiVO_4$ films depend critically on their synthesis methods such as spray pyrolysis,[9] electrodeposition[10] and metal−organic decomposition.[11−14] In addition, formation of the heterojunction structures has been demonstrated to improve the efficiency markedly in systems such as $BiVO_4/Co_3O_4$,[15] $BiVO_4/CuWO_4$[16] and $WO_3/BiVO_4$.[17,18] Introduction of the oxygen evolving cocatalyst is another way to improve the performance of semiconductor photocatalysts in photoelectrochemical water oxidation.[19] Thus, it was reported that loading "cobalt phosphate (Co-Pi)" containing cobalt oxide and hydroxide[20] on to the surface of $BiVO_4$ photoanode enhanced the efficiency significantly by reducing the recombination of electrons and holes.[14,16,21] Choi et al.[10] reported that iron oxyhydroxide (FeOOH) acted as an oxygen evolution catalyst and $BiVO_4$/FeOOH photoanode exhibited increased photocurrent for oxidation of water. All these efforts to improve the efficiency of photoanode are related to the reduced recombination and accelerated separation of electrons and holes. Recently, highly active $BiVO_4$-based photoanodes have been reported that employ multiple modifications.[22−24]

In an effort to improve the photocatalytic properties $BiVO_4$ in photoelectrochemical water oxidation, here we fabricated a heterojunction electrode between $BiVO_4$ and $CaFe_2O_4$. $CaFe_2O_4$ is a *p*-type oxide semiconductor and our favorite component to fabricate the heterojunction particulate photocatalysts such as $CaFe_2O_4/MgFe_2O_4$[25] and $CaFe_2O_4/$

Received: July 2, 2014
Accepted: September 18, 2014
Published: September 18, 2014

$PbBi_2Nb_{1.9}W_{0.1}O_9$,[26] or a photoanode like $CaFe_2O_4$/TaON.[27] Its valence band edge is more positive than the water oxidation potential, and both the conduction band and valence band are more negative than those of $BiVO_4$.[28] Therefore, these two semiconductors form staggered Type II relative band positions, as required to form an effective heterojunction photoanode. Thus, the $BiVO_4$ photoanode was first fabricated by the metal−organic decomposition method (MOD)[29] and particles of calcium ferrite were electrophoretically deposited[30] to construct a heterojunction photoanode. This heterojunction of $BiVO_4$/$CaFe_2O_4$ showed the increased photocatalytic activity and stability relative to the pristine $BiVO_4$ film in photoelectrochemical water oxidation under simulated 1 sun (100 mW cm^{-2}) irradiation. The origin of the enhancement by the heterojunction formation with $CaFe_2O_4$ was investigated in detail by applying H_2O_2 as a hole scavenger to study the yield of photogenerated holes that were successfully injected into the water oxidation reaction.

2. EXPERIMENTAL SECTION

2.1. Fabrication of Photoanodes and Characterizations. Bismuth vanadate ($BiVO_4$) was directly grown on the conducting substrate by the metal−organic decomposition method as described in our previous report.[29] Solutions of 0.2 M $Bi(NO_3)\cdot 5H_2O$ (Aldrich, 99.5%) in acetic acid (Kanto Chemicals, 99.7%) and 0.03 M $VO(acac)_2$ (Aldrich, 98.9%) in acetylacetonate (Kanto Chemicals, 99.5%) were mixed ultrasonically in the stoichiometric amounts for 30 min. The spin coating of the precursor solution onto F-doped SnO_2 glass (FTO, TEC-8, Pilkington) was conducted with the speed of 600 rpm for 30 s for a single layer coating, and the calcination in air at 440 °C for 30 min was followed. The spin coating/calcination process was repeated for eight times to obtain optimum thickness of the film and the final calcination was conducted at 470 °C for 5 h.

Calcium ferrite was synthesized by a conventional solid-state reaction. A mixture of $CaCO_3$ (Wako Pure Chemicals, 99.99%) and Fe_2O_3 (Wako Pure Chemicals, 99.9%) was ground in an agate mortar in the presence of ethanol for 30 min and calcined at 1100 °C for 5 h. The synthesized $CaFe_2O_4$ powder was deposited on top of the fabricated $BiVO_4$ electrode by electrophoretic deposition. The $CaFe_2O_4$ powder (40 mg) was dispersed in acetone (50 mL) with iodine (10 mg, Sigma-Aldrich, ≥99.8%). The $BiVO_4$ electrode ($BiVO_4$ coated area of 1 × 1 cm) and a clean FTO glass were immersed in the solution in parallel at a distance of 2 cm and 20 V was applied between the electrodes for 10 s using a DC power supply. After the electrode was rinsed with ethanol, the electrode was heat treated in air at 400 °C for 30 min to obtain the $BiVO_4$/$CaFe_2O_4$ electrode.

The obtained powders and fabricated films were characterized by an X-ray diffractometer (X'Pert PRO MPD, PANalytical) with a monochromated Cu Kα radiation (λ = 1.540 56 Å) at 40 kV and 30 mA and an UV−vis diffuse reflectance spectrophotometer (UV-2401PC, Shimadzu) with an integrating sphere (ISR-240A, Shimadzu). The scanning electron microscopy (SEM) images were obtained by field emission (FE)-SEM (JEOL JSM-7401F, JEOL).

2.2. Photoelectrochemical Measurements. Photoelectrochemical measurements were conducted in a three-electrode system with a potentiostat (Iviumstat, Ivium Technologies). The fabricated electrode, a platinum mesh and the Ag/AgCl electrode were used as the working, counter and reference electrodes, respectively. The cell was made of quartz glass, and 0.5 M sodium sulfate (pH 6.5) was used as an electrolyte after saturation with nitrogen gas for 30 min. The solar simulator (100 mW cm^{-2}, Model 91160, Oriel) equipped with an air mass (AM) 1.5G filter was used. The light intensity was calibrated to AM 1.5G by using a reference cell certified by the National Renewable Energy Laboratories, USA. The photocurrent was measured by linear sweep voltammetry from −0.4 to +1.2 V (vs Ag/AgCl) with a scan rate of 0.05 V s^{-1}. The light irradiation came from the backside of fluorine doped tin oxide (FTO) glass for all cases.

The hydrogen and oxygen evolution by photoelectrochemical water splitting was conducted in the airtight reactor connected to a closed gas circulation system. The 500 W Hg lamp (Hg Arc lamp source, Model 66902, Oriel) equipped with a liquid infrared (IR) filter (Water filter, Model 61945, Oriel) and a cutoff filter ($\lambda \geq 400$ nm, long pass filter, Model 59472, Oriel) was used to irradiate only visible light. The amount of hydrogen or oxygen was determined by a gas chromatography instrument equipped with a thermal conductivity detector (TCD) (HP 6890, molecular sieve 5 Å column, Ar carrier gas).

Incident photon to current conversion efficiency (IPCE) was measured in 0.5 M Na_2SO_4 of pH 6.5 at 1.23 V_{RHE} (RHE, reversible hydrogen electrode) under the irradiation of the 300 W Xe lamp (Xe Arc lamp source, Model 66905, Oriel) with a liquid IR filter (water filter, Model 61945, Oriel) and a monochromator (Oriel Cornerstone TM 130) with a bandwidth of 5 nm. The cutoff filter ($\lambda \geq 299$ nm, long pass filter, Model 59425, Oriel) was placed at the exit to prevent $\lambda/2$ radiation originated by Bragg diffraction at the grating. The incident light intensity was measured using a radiant power meter (Model 70260, Oriel) with a photodiode detector (Model 70282, Oriel).

2.3. Loading of Oxygen Evolving Catalyst. An oxygen evolving catalyst, cobalt phosphate (Co-Pi), was loaded by the photoassisted electrodeposition in a three-electrode system by the method reported elsewhere.[14,31] The fabricated electrode, a platinum mesh and Ag/AgCl were used as the working, counter and reference electrodes, respectively. The electrolyte solution was 0.5 mM cobalt nitrate hexahydrate in 0.1 M, pH 7 potassium phosphate (KPi) buffer. The electrodeposition was conducted by applying 0.5 V vs RHE for 5 min. After deposition of the cocatalyst, the electrodes were washed with distilled water and used to measure photocurrent generation. The electrolyte for the photoelectrochemical cell was also 0.1 M KPi buffered to pH 7.

3. RESULTS AND DISCUSSION

3.1. Physical Characterization of Photocatalysts and Photoanodes. The bismuth vanadate ($BiVO_4$) electrodes were fabricated by a metal−organic decomposition (MOD) method as described in our previous report.[29] Calcium ferrite ($CaFe_2O_4$) powder was synthesized by solid-state reaction and loaded onto the preformed $BiVO_4$ electrodes by electrophoretic deposition to form $CaFe_2O_4$/$BiVO_4$ heterojunction electrodes. X-ray diffraction (XRD) patterns of the two electrodes are shown in Figure 1. The peaks for SnO_2 from the FTO substrate were dominant for all cases as marked. The diffraction peaks from $BiVO_4$ could be assigned to a monoclinic structure (JCPDS No. 1-75-1867, space group = $I2/b$; a = 5.1956, b = 5.0935, c = 11.7044 Å) as shown in Figure 1a. In the case of the $CaFe_2O_4$/$BiVO_4$ heterojunction electrode, weak peaks from $CaFe_2O_4$ were observed although some were superposed onto

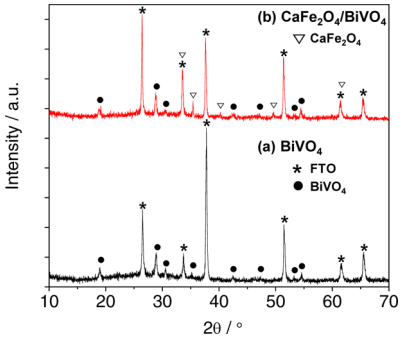

Figure 1. XRD patterns of (a) $BiVO_4$ and (b) $CaFe_2O_4$/$BiVO_4$ electrodes.

the strong SnO_2 peaks as shown in Figure 1b. The weak peaks were due to the sparse distribution of $CaFe_2O_4$ on $BiVO_4$ as discussed later with the SEM images. The XRD pattern of $CaFe_2O_4$ powder was also consistent with its orthorhombic structure (JCPDS No. 32-0168, space group = *Pnam*; a = 9.228, b = 10.705, c = 3.018 Å) as shown in Figure S1 of the Supporting Information.

Figure 2 shows the UV−visible absorption spectrum of $BiVO_4$ and $CaFe_2O_4/BiVO_4$ on the FTO substrate. The $BiVO_4$

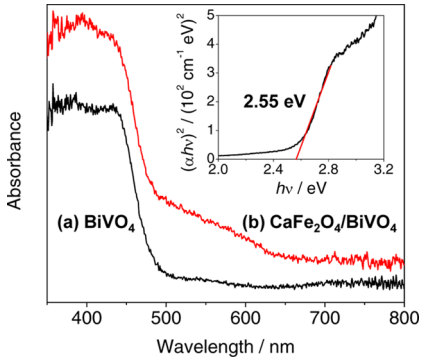

Figure 2. UV−vis absorption spectrum of (a) $BiVO_4$ and (b) $CaFe_2O_4/BiVO_4$ electrodes. The optical band gap of $BiVO_4$ was obtained by the Tauc plot, as shown in the inset.

electrode exhibited absorption in the visible light region with the absorption edge about 500 nm as shown in Figure 2a. The absorption of the $CaFe_2O_4/BiVO_4$ electrode in Figure 2b showed a gentle slope around 650 nm originated from the indirect band gap of $CaFe_2O_4$ (1.9 eV) and sharp increase around 490 nm due to the direct band gap of $BiVO_4$ (2.55 eV). Thus, the absorption spectrum of the $CaFe_2O_4/BiVO_4$ electrode represents a simple addition of individual spectra of $BiVO_4$ and $CaFe_2O_4$ (Figure S2 of the Supporting Information).

The morphology of electrodes was investigated by scanning electron microscopy (SEM) in Figure 3. The surface of the $BiVO_4$ electrode was porous and consisted of small grains about tens of nanometers, as shown in Figure 3a. The cross section SEM image in Figure 3b also showed a highly porous but well-

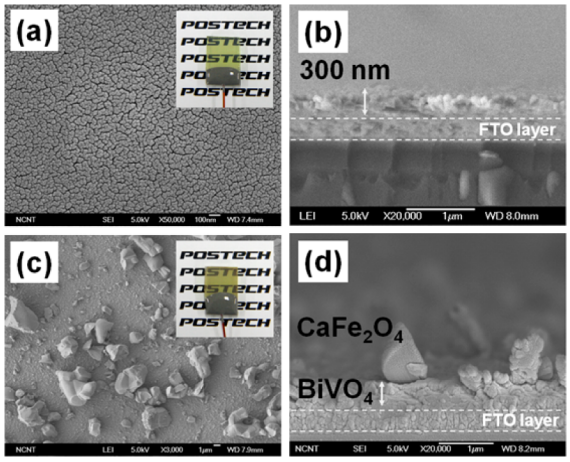

Figure 3. SEM images of (a,b) $BiVO_4$ and (c,d) $CaFe_2O_4/BiVO_4$ electrode: (a,c), top view; (b,d), side view. Insets demonstrate the transparency of the photoanodes.

connected $BiVO_4$ layer of around 300 nm thickness. The porosity allows facile penetration of electrolyte to contact the semiconductor and the particle connection is essential for uninterrupted interparticle electron transfer. The MOD method is thus effective to fabricate a uniform layer of highly crystalline $BiVO_4$. After electrophoretic deposition of $CaFe_2O_4$, its particles of several micrometers were observed on top of the $BiVO_4$ film, as shown in Figure 3c,d. Its coverage on the film was rather small for this optimal loading (Figure S3 of the Supporting Information). The optical transmittance of $BiVO_4$ and $CaFe_2O_4/BiVO_4$ on FTO was measured to be ca. 80% and ca. 50%, respectively, in 500−800 nm, as shown in Figure S4 (Supporting Information) and Figure 3 (insets). Thus, another advantage of the MOD method is to produce highly transparent films. The transparency was maintained even after the deposition of $CaFe_2O_4$. The transparent electrode is essential for fabrication of a tandem PEC cell with a photovoltaic device that provides bias potential using unused low energy part of the solar light.

3.2. Photoelectrochemical Performance of Photoanodes. Figure 4A shows that both $BiVO_4$ and $CaFe_2O_4/BiVO_4$ electrodes generate anodic photocurrents in 0.5 M Na_2SO_4 under the illumination of a solar simulator (AM 1.5G, 100 mW cm^{-2}). The bare $BiVO_4$ electrode showed a photocurrent density of 0.58 mA cm^{-2} at 1.23 V vs RHE. The photocurrent density will be compared at this potential hereafter, which is the standard reversible potential for water oxidation. This is quite a high photocurrent obtained from a bare $BiVO_4$ electrode, demonstrating that the MOD method is an efficient way to fabricate a highly active $BiVO_4$ film. The $CaFe_2O_4/BiVO_4$ heterojunction photoanode showed a photocurrent density of 0.96 mA cm^{-2}, or about 65% increase as compared to bare $BiVO_4$. The $CaFe_2O_4$ particles were deposited by electrophoretic deposition by applying 20 V for 10 s. The deposition time of $CaFe_2O_4$ was optimized for highest photocurrent generation, as shown in Figure S3 (Supporting Information). The shorter deposition time gave a sparser distribution of $CaFe_2O_4$ on $BiVO_4$ whereas the longer deposition time resulted in a higher coverage of the $BiVO_4$ surface by $CaFe_2O_4$, and both showed lower photocurrent densities than the optimized one.

In addition to the increased photocurrent in general, the $CaFe_2O_4/BiVO_4$ heterojunction photoanode exhibited an improved photocurrent response when the applied potential was low (from 0.2 to 0.7 V), lowering the onset voltage of photocurrent generation by ca. 0.1 V. It indicates that the water oxidation occurs more efficiently on the surface of $CaFe_2O_4/BiVO_4$ than $BiVO_4$. Chopped light chronoamperometry was measured to compare the transient photocurrent responses due to the dynamics of water oxidation, as shown in Figure 4B. The photocurrent was recorded for 10 s for each applied potential from 0.2 to 1.4 V (vs RHE) with 0.1 V steps. The $CaFe_2O_4/BiVO_4$ electrode showed higher photocurrent density than $BiVO_4$, especially in the low bias region from 0.3 to 0.5 V in the same manner as in Figure 4A. All the responses show the positive current transients of different magnitudes upon turning the light on. The transient represents the accumulation of holes at the electrode/electrolyte interface without injection to the electrolyte. The $BiVO_4$ electrode showed the high spike of the current, particularly at low potentials, indicating the presence of a high injection barrier. This photocurrent transient decreases over the $CaFe_2O_4/BiVO_4$ heterojunction photoanode by lowering the barrier. The charge separation of photogenerated

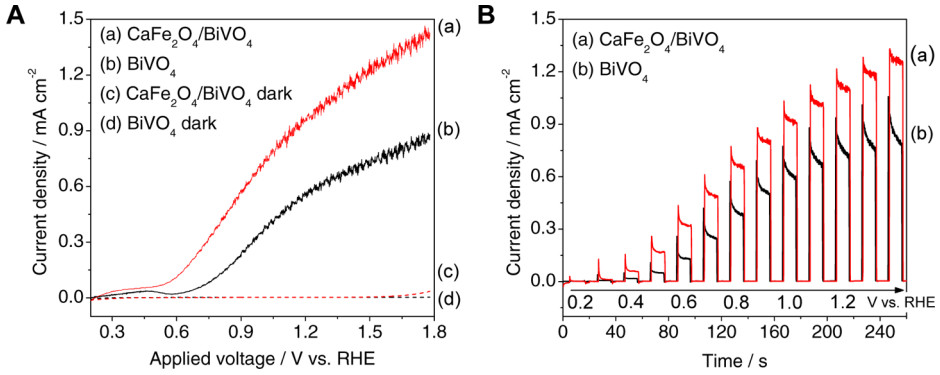

Figure 4. Photocurrent density vs applied voltage (A) and transient photocurrent density (B) of (a) $CaFe_2O_4/BiVO_4$ and (b) $BiVO_4$ electrode in 0.5 M Na_2SO_4 of pH 6.5 under AM 1.5G solar simulator irradiation. In panel B, the photocurrent was recorded for 10 s for each applied potential from 0.2 to 1.4 V (vs RHE) with the interval of 0.1 V. The dark currents of (a) and (b) are indicated in (c) and (d), respectively.

electrons and holes could be facilitated by $CaFe_2O_4/BiVO_4$ heterojunction relative to charge accumulation at the surface.

The incident photon to current efficiency (IPCE) was calculated by measuring the photocurrent under monochromatic light at 1.23 V vs RHE according to the following equation:

$$\mathrm{IPCE}(\%) = ([1240 \times J]/[\lambda \times P_{\mathrm{mono}}]) \times 100$$

where J is photocurrent density (mA cm^{-2}), λ is wavelength of incident light (nm) and P_{mono} is light power density of monochromated light (mW cm^{-2}). The IPCE values of $BiVO_4$ and $CaFe_2O_4/BiVO_4$ are about 5−10% and 20−22%, respectively, at 340−450 nm, as shown in Figure 5. The higher

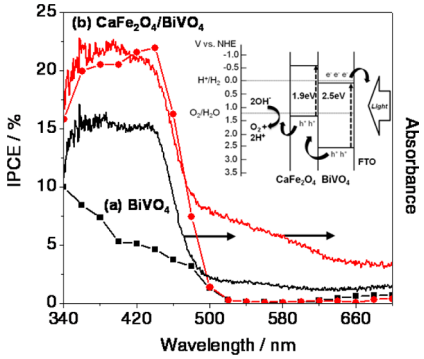

Figure 5. IPCE of (a) $BiVO_4$ and (b) $CaFe_2O_4/BiVO_4$ electrodes and their absorption spectra. Inset shows the energy diagram and expected charge flow of $CaFe_2O_4/BiVO_4$ heterojunction photoanode.

IPCE value of $CaFe_2O_4/BiVO_4$ demonstrates that the heterojunction electrode has transformed the photoexcited electrons and holes successfully to the photoelectrochemical water oxidation activity with much less efficiency loss. The IPCE values for both electrodes started to increase around 500 nm, corresponding to the band gap energy of $BiVO_4$ (2.55 eV) even in the presence of $CaFe_2O_4$, which has a smaller band gap energy (1.9 eV) with strong absorption up to 650 nm (Figure S2, Supporting Information). It indicates that the charge carriers generated in $CaFe_2O_4$ at the wavelength of 500−650 nm have contributed little to the photocurrent generation. The absorption in this range is due to indirect d-d transition by Fe^{3+} ions and the electrons and holes formed by this absorption are highly localized in Fe atom and tend to recombine easily.[28,32] Thus, the apparent role of heterojunction structure formed by $CaFe_2O_4/BiVO_4$ is to promote the separation of the photoexcited charge carriers generated mainly in $BiVO_4$ with little impact on the range of light absorption. This role is similar to that of $CaFe_2O_4$/TaON.,[27] yet disinguished from that of $WO_3/BiVO_4$ among heterojunction photoanodes that we studied.

The working principle of this heterojunction electrode is illustrated in terms of an energy diagram, as presented in the inset of Figure 5. The light is irradiated from the backside of the FTO substrate and absorbed by $BiVO_4$ first and then by $CaFe_2O_4$ for better utilization of incident solar light because the band gap of $CaFe_2O_4$ is smaller than that of $BiVO_4$. Thus, the $CaFe_2O_4/BiVO_4$ heterojunction photoanode can absorb a little more visible light than the single-component $BiVO_4$ photoanode. The high transmittance of $BiVO_4$ (80% in 500−800 nm) is also helpful for this cascade absorption of the light. Thus, photoexcited holes from $BiVO_4$ migrate to $CaFe_2O_4$ by the potential difference of two semiconductors. Electrons also move toward the FTO substrate from $CaFe_2O_4$ through $BiVO_4$ in the same manner. The different paths of electrons and holes are expected to reduce their recombination on the heterojunction photoanode and improve its activity for photoelectrochemical water oxidation.

3.3. Investigation of the Charge Separation on the Surface of Photoanode Using H_2O_2 as a Hole Scavenger.

As shown, the formation of the $CaFe_2O_4/BiVO_4$ heterojunction brings notable improvement in photocurrent generation due to the improved water oxidation activity. According to the operating principle of the heterojunction described above, the improvement originates from the efficient charge separation and reduced electron−hole recombination. The recombination could happen in the bulk or on the surface of the semiconductor. The effect of the heterojunction structure on the surface recombination could be investigated by introducing an easily oxidized hole scavenger in the water oxidation reaction that eliminates the injection barrier for holes. Hydrogen peroxide (H_2O_2) is a suitable hole scavenger because the structure is similar to water (H_2O) and the oxidation kinetics is faster than water by about 10 times.[14,33,34] It also has a low reduction potential (E° = 0.68 V vs RHE for O_2/H_2O_2) compared to 1.23 V for H_2O. The anodic photocurrent is generated by oxidation of H_2O_2:

$$H_2O_2 + 2h^+ \rightarrow 2H^+ + O_2$$

Thus, the photoelectrochemical H_2O_2 oxidation was performed over $BiVO_4$ and $CaFe_2O_4/BiVO_4$ photoanodes in 0.5 M Na_2SO_4 mixed with 0.25 mM H_2O_2 (35%, Junsei).

dx.doi.org/10.1021/am504283t | ACS Appl. Mater. Interfaces 2014, 6, 17762−17769

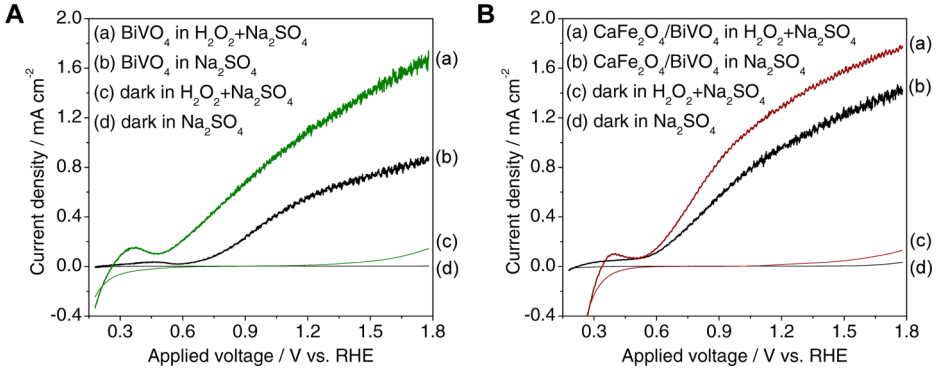

Figure 6. Photocurrent density under AM 1.5G solar simulator irradiation: (A) $BiVO_4$ in (a) H_2O_2/Na_2SO_4 and (b) Na_2SO_4. (B) $CaFe_2O_4/BiVO_4$ in (a) H_2O_2/Na_2SO_4 and (b) Na_2SO_4.

Figure 6A shows the photocurrent generated from $BiVO_4$ with and without H_2O_2. The presence of H_2O_2 increased the photocurrent from 0.58 to 1.14 mA cm^{-2} and onset of current generation shifted from 0.6 V to a lower bias potential of 0.5 V. The result could be understood by the known role of the hole scavenger H_2O_2 that promotes the injection of holes to the electrolyte interface for water oxidation reaction. In general, the surface recombination of photoexcited electrons and holes is dominant in the low bias potential region and hinders the transfer of charge carriers. But H_2O_2 used as a hole scavenger effectively eliminates the hole injection barrier and surface recombination.[33]

Now the same hole scavenger experiments were carried out for heterojunction $CaFe_2O_4/BiVO_4$ photoanodes, as shown in Figure 6B. The photocurrent generated from the oxidation of H_2O_2 on $CaFe_2O_4/BiVO_4$ was 1.33 mA cm^{-2} whereas that of water was 0.96 mA cm^{-2}. The increase of photocurrent due to H_2O_2 addition was not as much as that of $BiVO_4$. In addition, unlike the $BiVO_4$ electrode, the photocurrents were similar around 0.5 V with and without H_2O_2, and there was no change in current onset potential either. Thus, it appears that the heterojunction of $CaFe_2O_4/BiVO_4$ has promoted the transfer of holes to the electrode/electrolyte interface at the low bias potential region without H_2O_2. For direct comparison, the transient photocurrents of all cases are plotted in Figure 7. The transient photocurrents exhibited the following trend: $BiVO_4$ without H_2O_2 (d) < $CaFe_2O_4/BiVO_4$ without H_2O_2 (c) < $BiVO_4$ with H_2O_2 (b) < $CaFe_2O_4/BiVO_4$ with H_2O_2 (a). The difference between $CaFe_2O_4/BiVO_4$ and $BiVO_4$ in the presence of H_2O_2 disappeared at the higher bias region (>1.1 V_{RHE}). Thus, the formation of the heterojunction with $CaFe_2O_4$ improved the rate of water oxidation reactions over $BiVO_4$, probably by efficient injection of holes to the electrolyte over the entire potential range. The photocurrent generation on $CaFe_2O_4/BiVO_4$ was close to that of $BiVO_4$ with H_2O_2 with almost 100% injection yield. Moreover, the photocurrent decay upon chopped illumination on $CaFe_2O_4/BiVO_4$ became slower relative to that of $BiVO_4$, indicating the improved hole injection yield. Thus, the role of $CaFe_2O_4$ particles deposited on $BiVO_4$ is to enhance the hole injection into the semiconductor–electrolyte interface for water oxidation. It could be achieved from the facile transfer of photoexcited electrons and holes to FTO and electrode/electrolyte interface, respectively, according to the band structure of the heterojunction, as shown in the inset of Figure 5.

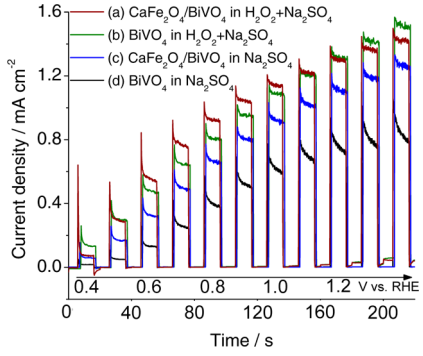

Figure 7. Transient photocurrent density of (a) $CaFe_2O_4/BiVO_4$ electrodes in H_2O_2/Na_2SO_4, (b) $BiVO_4$ in H_2O_2/Na_2SO_4, (c) $CaFe_2O_4/BiVO_4$ in Na_2SO_4 and (d) $BiVO_4$ in Na_2SO_4 under chopped illumination of solar simulator (AM 1.5G). The photocurrent was recorded for 10 s for each applied potential from 0.4 to 1.4 V (vs RHE) with the interval of 0.1 V.

For more quantitative discussion, we can extract the injection yield of holes from data in Figures 6 and 7 using the following equation:[33]

$$J_{\text{photocurrent}}^{\text{H2O}} = J_{\text{absorbed}} \times P_{\text{charge separation}} \times P_{\text{charge injection}}$$

where $J_{\text{photocurrent}}^{\text{H2O}}$ or photocurrent by water oxidation is expressed as the product of the rate of photon absorption (J_{absorbed}), the charge separation yield ($P_{\text{charge separation}}$), and the charge injection yield to electrolyte ($P_{\text{charge injection}}$). The charge separation yield is related to the recombination in the bulk of the main light absorber ($BiVO_4$ in the present case), whereas the charge injection yield represents the fraction of the holes that reach the electrode/electrolyte interface and participate in water oxidation reaction avoiding surface recombination. Since the charge injection yield of H_2O_2 is almost 100% ($P_{\text{charge injection}} = 1$),[33] the photocurrent from its oxidation can be expressed by the following equation:

$$J_{\text{photocurrent}}^{\text{H2O2}} = J_{\text{absorbed}} \times P_{\text{charge separation}}$$

Thus, the charge injection yield can be obtained simply by the following equation:

$$P_{\text{charge injection}} = J_{\text{photocurrent}}^{\text{H2O}} / J_{\text{photocurrent}}^{\text{H2O2}}$$

As shown in Figure 8A, the hole injection yield of the $BiVO_4$ photoanode remained below 50%, indicating that the more than half of the generated holes are wasted by recombination on the surface instead of contributing to the water oxidation

dx.doi.org/10.1021/am504283t | ACS Appl. Mater. Interfaces 2014, 6, 17762–17769

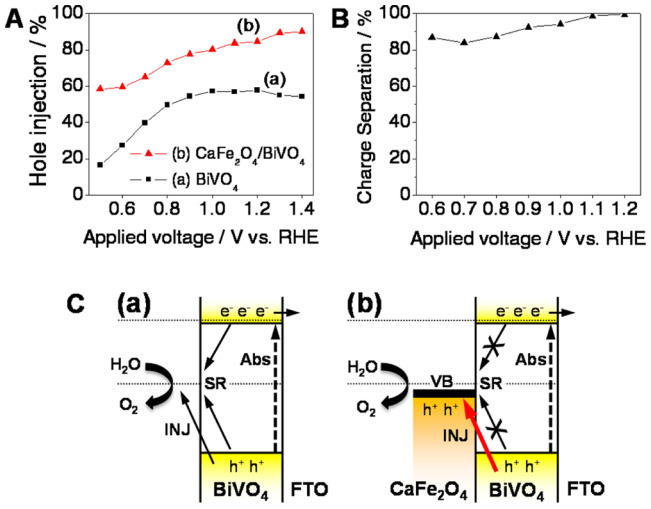

Figure 8. (A) Hole injection yield of (a) $BiVO_4$ and (b) $CaFe_2O_4$/$BiVO_4$ photoanodes. (B) Relative charge separation yield $P_{\text{charge separation}}$ between $BiVO_4$ and $CaFe_2O_4$/$BiVO_4$ photoanodes. (C) Schematic diagrams illustrating the reaction at the surface of (a) $BiVO_4$ and (b) $CaFe_2O_4$/$BiVO_4$ photoanodes. (Abs: photon absorption and charge carrier generation. SR: surface recombination. INJ: hole injection into electrode/electrolyte interface.)

reaction. The hole injection yield of the $CaFe_2O_4$/$BiVO_4$ photoanode started from 60% at 0.5 V, became 80% at 1.2 V and reached 90% above 1.3 V. The situation is illustrated in Figure 8C. The electrons and holes that are generated by photon absorption and survive the bulk recombination process can easily recombine at the surface of the $BiVO_4$ photoanode. On the other hand, the valence band of $CaFe_2O_4$ lies at a much higher potential (more negative) than that of $BiVO_4$ and just below water oxidation potential (1.23 V_{RHE}). Thus, it can act as a stepping stone to transfer holes generated from $BiVO_4$ to the electrode/electrolyte interface. Thus, the surface recombination is greatly reduced by the formation of the $CaFe_2O_4$/$BiVO_4$ heterojunction and the holes could be injected successfully into electrolyte to participate in the water oxidation reaction, as demonstrated by the increase of the hole injection yield. The relative charge separation yield between $BiVO_4$ and $CaFe_2O_4$/$BiVO_4$ was also obtained by dividing J^{H2O2}_{BiVO4} by $J^{H2O2}_{CaFe2O4/BiVO4}$, as shown in Figure 8B. It showed about 90%, even at the low bias potential region and reached 100% at 1.1 V_{RHE}. As shown in Figure 2, the absorbances of the two electrodes are almost the same, except for the small shoulder at 500−650 nm for $CaFe_2O_4$/$BiVO_4$. Direct comparison of these absorbance spectra with AM 1.5G radiation spectrum gives J_{abs} of ∼3.4 mA/cm^2 for bare $BiVO_4$ and ∼3.6 mA/cm^2 for $CaFe_2O_4$/$BiVO_4$. Then, the similar values of J^{H2O2}_{BiVO4} and $J^{H2O2}_{CaFe2O4/BiVO4}$ indicate that the bulk recombination has occurred to the almost the same extent in both photoanodes, and $CaFe_2O_4$ reduces only the surface recombination on $BiVO_4$ layer.

3.4. Effect of Oxygen Evolving Catalysts. An oxygen evolving catalyst, cobalt phosphate (Co-Pi) has been widely employed for semiconductor photoanodes since its activity was first reported for water oxidation.[19] It contains cobalt oxide and hydroxide species and shows the catalytic effect effectively in a neutral phosphate buffer solution.[35] Thus, Co-Pi was loaded on both $BiVO_4$ and $CaFe_2O_4$/$BiVO_4$ photoanodes by a photo-assisted electrodeposition method[31] by applying 0.5 V vs RHE for 5 min in the electrolyte solution of 0.5 mM cobalt nitrate hexahydrate in 0.1 M pH 7 potassium phosphate (KPi) buffer.

As shown in Figure 9A, the Co-Pi/$BiVO_4$ photoanode showed the improved photocurrent density of 0.76 mA cm^{-2} at 1.23 V vs RHE, which represents a significant improvement over that of bare $BiVO_4$ (0.58 mA cm^{-2}). In comparison with the $CaFe_2O_4$/$BiVO_4$ heterojunction electrode in Figure 4A(a), the photocurrent density was lower (vs 0.96 mA cm^{-2} in 0.5 M Na_2SO_4), but the cathodic shift of the onset potential was almost the same. When Co-Pi was added to $CaFe_2O_4$/$BiVO_4$, the photocurrent density of Co-Pi/$CaFe_2O_4$/$BiVO_4$ became 0.9 mA cm^{-2}, similar to that of $CaFe_2O_4$/$BiVO_4$, but there was an additional onset potential shift, shown in Figure 9A(a). Thus, the effects of heterojunction formation and oxygen evolving cocatalyst loading on $BiVO_4$ appear very similar; increasing the photocurrent generation and making a cathodic shift of current onset potential. Of course, they work on different principles; Co-Pi utilizes the redox cycles of cobalt ions to accelerate water oxidation kinetics, whereas heterojunction utilizes difference in valence band positions for hole transfer. But they show the similar effects because both lead to the reduced charge recombination on the $BiVO_4$ surface. As mentioned, loading Co-Pi on $CaFe_2O_4$/$BiVO_4$ brings an additional shift of onset potential, indicating that Co-Pi can add its own functionality on the $CaFe_2O_4$/$BiVO_4$ heterojunction system.

As shown in Figure S5 (Supporting Information), it was also found that Co-Pi improved the stability of the photoanode.

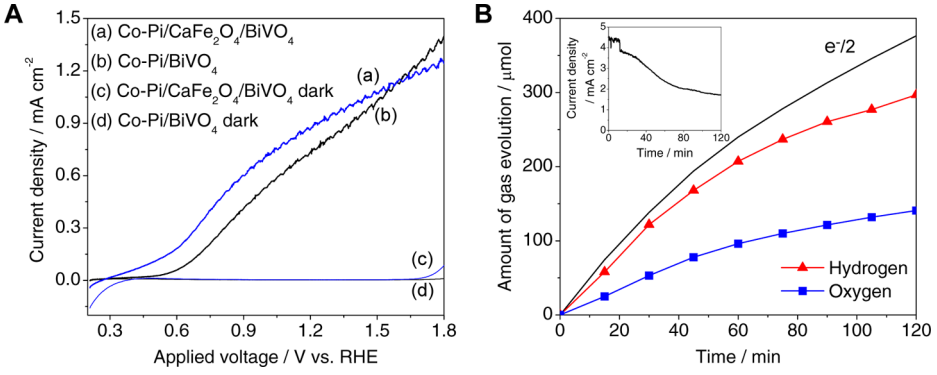

Figure 9. (A) Photocurrent density of (a) Co-Pi/$CaFe_2O_4$/$BiVO_4$ and (b) Co-Pi/$BiVO_4$ electrode in 0.1 M potassium phosphate (KPi) buffered at pH 7 under AM 1.5G solar simulator irradiation. (B) Hydrogen and oxygen evolution for Co-Pi/$CaFe_2O_4$/$BiVO_4$ electrode in 0.1 M potassium phosphate (KPi) of pH 7 in three electrode system under visible light irradiation (λ > 400 nm). The applied bias was 1.3 V vs RHE. The expected amount of hydrogen molecules, $e^-/2$, is presented as a solid line. The inset shows time course of photocurrent generation.

dx.doi.org/10.1021/am504283t | ACS Appl. Mater. Interfaces 2014, 6, 17762−17769

Thus, the transient photocurrent density over $CaFe_2O_4/BiVO_4$ in 0.5 M Na_2SO_4 (same condition as Figure 4A) decreased continuously for 15 min of irradiation, whereas Co-Pi/$CaFe_2O_4/BiVO_4$ in 0.1 M potassium phosphate of pH 7 did not show any significant decay of the photocurrent generation. The result indicates that the oxygen evolving catalyst is beneficial for stabilization of the $CaFe_2O_4/BiVO_4$ heterojunction photoanode. To find the reason for the poor stability, the surface of heterojunction film was observed by SEM before and after use of the $CaFe_2O_4/BiVO_4$ photoelectrode without Co-Pi. As shown in Figure S6 (Supporting Information), $CaFe_2O_4$ particles were detached from the $BiVO_4$ film during the reaction, resulting in a rapid drop to low photocurrents. A conspicuous role of Co-Pi seems to physically protect the heterojunction structure by covering up the structure.

The evolution of hydrogen and oxygen gases during the photoelectrochemical water splitting reaction was measured for Co-Pi/$CaFe_2O_4/BiVO_4$ in 0.1 M potassium phosphate of pH 7 under the illumination of visible light ($\lambda \geq 400$ nm, 500 W Hg lamp) to confirm that the generation of the current was mainly due to the water splitting reactions. The applied bias was 1.3 V vs RHE using the three electrode system in a closed circulation system to accumulate the produced gases. The total amount of oxygen and hydrogen evolved for 2 h was 140 μmol and 297 μmol, as shown in Figure 9B. Slightly more hydrogen was evolved than the stoichiometric ratio (H_2:O_2 = 2.1:1) due to the slow kinetics of oxygen evolution. The faradaic efficiency (actual gas evolution rates/those expected from current generation) during this reaction was about 78−88%, as presented in Table S1 (Supporting Information). The loss of faradaic efficiency for hydrogen and oxygen probably comes from the unwanted backward reaction with H_2 and O_2 or the slow kinetics of water oxidation, respectively. The time course of photocurrent generation is also presented in Figure 9B (inset). The photocurrent density was initially about 4 mA cm^{-2}, which dropped rapidly for the first 30 min and then decreased slowly after then. We postulate that the stability of $CaFe_2O_4/BiVO_4$ photoanode could be improved by developing a more efficient way to load the oxygen evolving catalyst. With the limitation, the results clearly show that Co-Pi/$CaFe_2O_4$/$BiVO_4$ could work as an efficient photoanode for the photoelectrochemical water splitting reaction.

4. CONCLUSIONS

The $CaFe_2O_4/BiVO_4$ heterojunction photoanode was fabricated by electrophoretic deposition of $CaFe_2O_4$ powder on the $BiVO_4$ electrode formed by a metal−organic decomposition method. The photocurrent density of the $CaFe_2O_4/BiVO_4$ heterojunction photoanode increased about 65% from that of bare $BiVO_4$. The origin of the increased photocurrent density was investigated using hydrogen peroxide as a hole scavenger. It was demonstrated that the heterojunction formation reduced the charge recombination on the electrode surface with little effect on bulk recombination. Thus, photogenerated holes are efficiently transferred into the electrode/electrolyte interface for facile water oxidation.

■ ASSOCIATED CONTENT

Supporting Information

XRD, UV−vis DRS and Tauc plots for $CaFe_2O_4$ powder; photocurrent density vs $CaFe_2O_4$ deposition time of $CaFe_2O_4$/$BiVO_4$ for optimization; optical transmittance of $BiVO_4$ and $CaFe_2O_4/BiVO_4$ on FTO substrate; chronoamperometry of $CaFe_2O_4/BiVO_4$ and Co-Pi/$CaFe_2O_4/BiVO_4$; faradaic efficiency of hydrogen and oxygen evolution for the Co-Pi/$CaFe_2O_4/BiVO_4$ electrode. This material is available free of charge via the Internet at http://pubs.acs.org.

■ AUTHOR INFORMATION

Corresponding Author

*J. S. Lee. E-mail: jlee1234@unist.ac.kr.

Author Contributions

§These authors contributed equally.

Notes

The authors declare no competing financial interest.

■ ACKNOWLEDGMENTS

This work was supported with the financial support by the Korea Center for Artificial Photosynthesis (KCAP) (No. 2009-0093880), Basic Science Research Program (No. 2012-017247), A3 Foresight program and BK+ program through the National Research Foundation of Korea (NRF) funded by the Ministry of Science, ICT and Creative Future Planning.

■ REFERENCES

(1) Fujishima, A.; Honda, K. Electrochemical Photolysis of Water at a Semiconductor Electrode. *Nature* **1972**, *238*, 37−38.

(2) Marsen, B.; Miller, E. L.; Paluselli, D.; Rocheleau, R. E. Progress in Sputtered Tungsten Trioxide for Photoelectrode Applications. *Int. J. Hydrogen Energy* **2007**, *32*, 3110−3115.

(3) Hong, S. J.; Jun, H.; Borse, P. H.; Lee, J. S. Size Effects of WO_3 Nanocrystals for Photooxidation of Water in Particulate Suspension and Photoelectrochemical Film Systems. *Int. J. Hydrogen Energy* **2009**, *34*, 3234−3242.

(4) Sivula, K.; Le Formal, F.; Grätzel, M. Solar Water Splitting: Progress Using Hematite (α-Fe_2O_3) Photoelectrodes. *ChemSusChem* **2011**, *4*, 432−449.

(5) Jun, H.; Im, B.; Kim, J. Y.; Im, Y. O.; Jang, J. W.; Kim, E. S.; Kim, J. Y.; Kang, H. J.; Hong, S. J.; Lee, J. S. Photoelectrochemical Water Splitting over Ordered Honeycomb Hematite Electrodes Stabilized by Alumina Shielding. *Energy Environ. Sci.* **2012**, *5*, 6375−6382.

(6) Iwase, A.; Kudo, A. Photoelectrochemical Water Splitting Using Visible-Light-Responsive $BiVO_4$ Fine Particles Prepared in an Aqueous Acetic Acid Solution. *J. Mater. Chem.* **2010**, *20*, 7536−7542.

(7) Kudo, A.; Omori, K.; Kato, H. A Novel Aqueous Process for Preparation of Crystal Form-Controlled and Highly Crystalline $BiVO_4$ Powder from Layered Vanadates at Room Temperature and Its Photocatalytic and Photophysical Properties. *J. Am. Chem. Soc.* **1999**, *121*, 11459−11467.

(8) Yin, W.-J.; Wei, S.-H.; Al-Jassim, M.; Turner, J.; Yan, Y. Doping Properties of Monoclinic $BiVO_4$ Studied by First-Principles Density-Functional Theory. *Phys. Rev. B: Condens. Matter Mater. Phys.* **2011**, *83*, 155102.

(9) Liang, Y.; Tsubota, T.; Mooij, L. P. A.; van de Krol, R. Highly Improved Quantum Efficiencies for Thin Film $BiVO_4$ Photoanodes. *J. Phys. Chem. C* **2011**, *115*, 17594−17598.

(10) Seabold, J. A.; Choi, K. S. Efficient and Stable Photo-Oxidation of Water by a Bismuth Vanadate Photoanode Coupled with an Iron Oxyhydroxide Oxygen Evolution Catalyst. *J. Am. Chem. Soc.* **2012**, *134*, 2186−2192.

(11) Sayama, K.; Nomura, A.; Zou, Z.; Abe, R.; Abe, Y.; Arakawa, H. Photoelectrochemical Decomposition of Water on Nanocrystalline $BiVO_4$ Film Electrodes under Visible Light. *Chem. Commun.* **2003**, *9*, 2908−2909.

(12) Pilli, S. K.; Furtak, T. E.; Brown, L. D.; Deutsch, T. G.; Turner, J. A.; Herring, A. M. Cobalt-Phosphate (Co-Pi) Catalyst Modified Mo-Doped $BiVO_4$ Photoelectrodes for Solar Water Oxidation. *Energy Environ. Sci.* **2011**, *4*, 5028−5034.

(13) Pilli, S. K.; Deutsch, T. G.; Furtak, T. E.; Turner, J. A.; Brown, L. D.; Herring, A. M. Light Induced Water Oxidation on Cobalt-Phosphate (Co-Pi) Catalyst Modified Semi-Transparent, Porous SiO_2-$BiVO_4$ Electrodes. *Phys. Chem. Chem. Phys.* **2012**, *14*, 7032−7039.
(14) Zhong, D. K.; Choi, S.; Gamelin, D. R. Near-Complete Suppression of Surface Recombination in Solar Photoelectrolysis by "Co-Pi" Catalyst-Modified W:$BiVO_4$. *J. Am. Chem. Soc.* **2011**, *133*, 18370−18377.
(15) Long, M.; Cai, W.; Cai, J.; Zhou, B.; Chai, X.; Wu, Y. Efficient Photocatalytic Degradation of Phenol over Co_3O_4/$BiVO_4$ Composite under Visible Light Irradiation. *J. Phys. Chem. B* **2006**, *110*, 20211−20216.
(16) Pilli, S. K.; Deutsch, T. G.; Furtak, T. E.; Brown, L. D.; Turner, J. A.; Herring, A. M. $BiVO_4$/$CuWO_4$ Heterojunction Photoanodes for Efficient Solar Driven Water Oxidation. *Phys. Chem. Chem. Phys.* **2013**, *15*, 3273−3278.
(17) Hong, S. J.; Lee, S.; Jang, J. S.; Lee, J. S. Heterojunction $BiVO_4$/WO_3 Electrodes for Enhanced Photoactivity of Water Oxidation. *Energy Environ. Sci.* **2011**, *4*, 1781−1787.
(18) Su, J.; Guo, L.; Bao, N.; Grimes, C. A. Nanostructured WO_3/$BiVO_4$ Heterojunction Films for Efficient Photoelectrochemical Water Splitting. *Nano Lett.* **2011**, *11*, 1928−1933.
(19) Kim, J. H.; Jang, J.-W.; Kang, H. J.; Magesh, G.; Kim, J. Y.; Kim, J. H.; Lee, J.; Lee, J. S. Palladium Oxide as a Novel Oxygen Evolution Catalyst on $BiVO_4$ Photoanode for Photoelectrochemical Water Splitting. *J. Catal.* **2014**, *317*, 126−134.
(20) Kanan, M. W.; Nocera, D. G. In Situ Formation of an Oxygen-Evolving Catalyst in Neutral Water Containing Phosphate and Co^{2+}. *Science* **2008**, *321*, 1072−1075.
(21) Zhou, M.; Bao, J.; Bi, W.; Zeng, Y.; Zhu, R.; Tao, M.; Xie, Y. Efficient Water Splitting Via a Heteroepitaxial $BiVO_4$ Photoelectrode Decorated with Co-Pi Catalysts. *ChemSusChem* **2012**, *5*, 1420−1425.
(22) Abdi, F. F.; Han, L.; Smets, A. H.; Zeman, M.; Dam, B.; van de Krol, R. Efficient Solar Water Splitting by Enhanced Charge Separation in a Bismuth Vanadate-Silicon Tandem Photoelectrode. *Nat. Commun.* **2013**, *4*, 2195.
(23) Kim, T. W.; Choi, K.-S. Nanoporous $BiVO_4$ Photoanodes with Dual-Layer Oxygen Evolution Catalysts for Solar Water Splitting. *Science* **2014**, *343*, 990.
(24) Rao, P. M.; Cai, L.; Liu, C.; Cho, I. S.; Lee, C. H.; Weisse, J. M.; Yang, P.; Zheng, X. Simultaneously Efficient Light Absorption and Charge Separation in WO_3/$BiVO_4$ Core/Shell Nanowire Photoanode for Photoelectrochemical Water Oxidation. *Nano Lett.* **2014**, *14*, 1099.
(25) Kim, H. G.; Borse, P. H.; Jang, J. S.; Jeong, E. D.; Jung, O.-S.; Suh, Y. J.; Lee, J. S. Fabrication of $CaFe_2O_4$/$MgFe_2O_4$ Bulk Heterojunction for Enhanced Visible Light Photocatalysis. *Chem. Commun.* **2009**, *39*, 5889.
(26) Kim, H. G.; Borse, P. H.; Choi, W.; Lee, J. S. Photocatalytic Nanodiodes for Visible-Light Photocatalysis. *Angew. Chem., Int. Ed.* **2005**, *44*, 4585−4589.
(27) Kim, E. S.; Nishimura, N.; Magesh, G.; Kim, J. Y.; Jang, J. W.; Jun, H.; Kubota, J.; Domen, K.; Lee, J. S. Fabrication of $CaFe_2O_4$/TaON Heterojunction Photoanode for Photoelectrochemical Water Oxidation. *J. Am. Chem. Soc.* **2013**, *135*, 5375−5383.
(28) Matsumoto, Y. Energy Positions of Oxide Semiconductors and Photocatalysis with Iron Complex Oxides. *J. Solid State Chem.* **1996**, *126*, 227−234.
(29) Parmar, K. P. S.; Kang, H. J.; Bist, A.; Dua, P.; Jang, J. S.; Lee, J. S. Photocatalytic and Photoelectrochemical Water Oxidation over Metal-Doped Monoclinic $BiVO_4$ Photoanodes. *ChemSusChem* **2012**, *5*, 1926−1934.
(30) Abe, R.; Higashi, M.; Domen, K. Facile Fabrication of an Efficient Oxynitride TaON Photoanode for Overall Water Splitting into H_2 and O_2 under Visible Light Irradiation. *J. Am. Chem. Soc.* **2010**, *132*, 11828−11829.
(31) Zhong, D. K.; Cornuz, M.; Sivula, K.; Grätzel, M.; Gamelin, D. R. Photo-Assisted Electrodeposition of Cobalt-Phosphate (Co-Pi) Catalyst on Hematite Photoanodes for Solar Water Oxidation. *Energy Environ. Sci.* **2011**, *4*, 1759−1764.
(32) Ida, S.; Yamada, K.; Matsunaga, T.; Hagiwara, H.; Matsumoto, Y.; Ishihara, T. Preparation of p-Type $CaFe_2O_4$ Photocathodes for Producing Hydrogen from Water. *J. Am. Chem. Soc.* **2010**, *132*, 17343−17345.
(33) Dotan, H.; Sivula, K.; Grätzel, M.; Rothschild, A.; Warren, S. C. Probing the Photoelectrochemical Properties of Hematite (α-Fe_2O_3) Electrodes Using Hydrogen Peroxide as a Hole Scavenger. *Energy Environ. Sci.* **2011**, *4*, 958−964.
(34) Itoh, K.; Bockris, J. O. M. Thin Film Photoelectrochemistry: Iron Oxide. *J. Electrochem. Soc.* **1984**, *131*, 1266−1271.
(35) Zhong, D. K.; Gamelin, D. R. Photo-Electrochemical Water Oxidation by Cobalt Catalyst ("Co-Pi")/α-Fe_2O_3 Composite Photoanodes: Oxygen Evolution and Resolution of a Kinetic Bottleneck. *J. Am. Chem. Soc.* **2010**, *132*, 4202−4207.